Available online at www.sciencedirect.com
SCIENCE DIRECT®
International Journal of Machine Tools & Manufacture 44 (2004) 307–316
INTERNATIONAL JOURNAL OF MACHINE TOOLS & MANUFACTURE DESIGN, RESEARCH AND APPLICATION
www.elsevier.com/locate/ijmatool

# Analysis and investigation of ballistic impact on ceramic/metal composite armour

D.P. Gonçalves [a], F.C.L. de Melo [a], A.N. Klein [b], H.A. Al-Qureshi [b,*]

[a] CTA-AMR, São José dos Campos, 12228-900, SP, Brazil
[b] Laboratório de Materiais, Dept Eng Mec, UFSC, CP 476, Florianópolis, SC 88040-900, Brazil

Received 27 August 2003; accepted 16 September 2003

**Abstract**

The subject of this paper is to analyze the impact of projectiles against ceramic/metal armour using a simple one-dimensional mode. The model allows the calculation of the loss of projectile mass and its velocity, and gives the deflection of the backup material. This work also investigates the influence of grain size of the ceramic material on ballistic performance, which is very useful during selection of the best material for each application. Therefore, two formulations of the same ceramic material were produced. They had the same chemical composition, the same mechanical properties, but different grain size. The ballistic performances were compared measuring the maximum velocity each formulation was able to support, without perforation.


*Keywords:* Ceramic composite; Armour; Ballistic impact; Safety

## 1. Introduction

Generally, impact problems were primarily of concern to the military, either for defenseive or offensive purposes to develop armour or ammunition. Nowadays, civilian applications demand extreme safety of the products, therefore, it is essential to understand the material behaviour under intense short duration or impact loadings [1]. Needless to say, using metallic armour for personal protection is extremely heavy and would not be popular. On the other hand, reinforced fiber composites have been used for these purposes, but have been shown to be very susceptible to impact damage, thus limiting their usefulness for such an application [2–4]. It is essential therefore that armour be as light as posssible for military operations requiring high manoeuvrability.

Certain high hardness ceramics combined with their low density offer the possibility of reducing the weight per unit area required for given protection. Needless to say, in these cases ceramic armour emerges as a rigid covering, capable of reducing the mass and the impact velocity of the projectile, causing it to disintegrate into small fragments which could easily be absorbed by the flexible base which supports the ceramic layer. The dynamic load of projectile impact on a target involves complex mechanism of penetration and perforation, thus making it necessary to introduce many simplifying assumptions to the problem. For such reasons, many experimental tests of different conditions of design, material, type of projectile and others are needed.

In the present work, several tests have been conducted at various impact velocities of projectiles and energy levels to characterize the projectile impact behaviour on ceramic–metal composites.

## 2. Simplified theoretical analysis

The mechanics of perforation of projectiles on metallic plates has already been analysed theoretically by many authors [2–12]. These types of analyses lead to the determination of the required impact perforation energy and the residual strength. In the present study,

* Corresponding author. Tel.: +55-48-331-9268; fax: +55-48-234-0059.
*E-mail address:* hazim@materiais.ufsc.br (H.A. Al-Qureshi).

0890-6955/$ - see front matter © 2003 Elsevier Ltd. All rights reserved.
doi:10.1016/j.ijmachtools.2003.09.005

the armour of composite material is made of two different materials having different properties, and they perform in a complementary manner during the process of perforation of the projectile. The ceramic material receives the initial impact of the projectile and its function is to destroy the head of the projectile progressively as it tries to penetrate the composite materials. In this initial stage a major part of the impact energy is dissipated. Then in the second stage the base layer is made of ductile material and its main function is to absorb the residual impact energy caused by the fragmented parts of the projectile as it comes to a complete halt, thus resulting in plastic deformation of the ductile material. A brief description of each stage will be presented.

### 2.1. First stage

The initial stage is the destruction of the head of the projectile without penetration of the ceramic layer, in addition to the formation of cracks in the form of a cone. During this stage, the impact of the projectile generates compressive shock waves which travel across the ceramic thickness. This wave will reflect back as a tension wave which tends to crack the ceramic and causes the fractured cone formation (Fig. 1). The angle of the cone (Fig. 1) depends on the elastic properties of the projectile and the ceramic plate. However, in quasi-static condition this angle is approximately equal to $68^{\circ}$. In the present work and due to the difficulties in estimating this angle during the ballistic impact, it was assumed to be $68^{\circ}$.

It is clearly shown in Fig. 2, that the effect of erosion on the projectile head ($7.62 \times 51$ mm) was caused by the impact on the ceramic plate, which was perforated at the end of this stage. It can also be seen that not only the complete destruction of the head of the projectile occurred, but also some evident cracks propagated longitudinally.

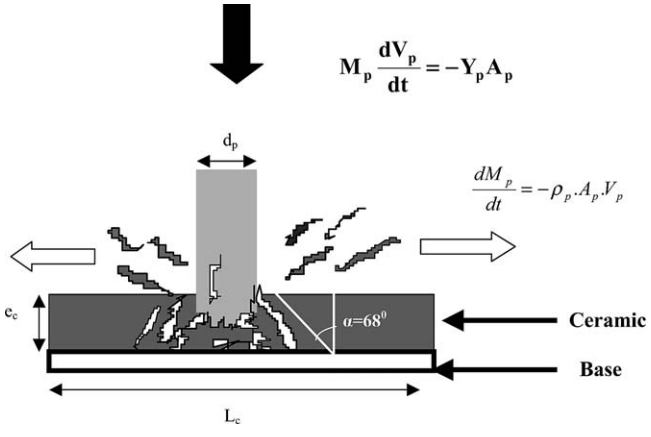


Fig. 1. First stage penetration into ceramic plate.

It is assumed that the time taken to form this cone is equal to $t = 6e_c/c$ [2], where $e_c$ is the thickness of the plate and $c$ is the longitudinal velocity of the sound. For the plates having 10 mm thickness, then the time required to form the fracture cone is approximately equal to 6 μs.

During the initial impact the rear velocity of the projectile is $V_p(t)$, whilst the interface ceramic-projectile velocity $V_i(t)$ is nil. Now to erode the head of the projectile then the dynamic yielding of the projectile material ($Y_p = 2.9$ HV) according to Tabor [13]) must be exceeded, then the force opposing penetration can be given as

$$M_p \frac{dV_p}{dt} = -Y_p A_p. \tag{1}$$

Needless to say the geometry of the projectile is governed by the following equation

$$\frac{dM_p}{dt} = -\rho_p A_p V_p. \tag{2}$$

### 2.2. Second stage

In this stage the projectile penetrates the armour and the fractured cone propagates causing lateral spread of the ceramic fragments (Fig. 3) and simultaneously the base of the armour starts to deform elastically. The velocity here can be divided into two regions, firstly, the rear part of the projectile continues to move at the velocity of $V_p(t)$, whereas the interface projectile-ceramic moves at a velocity of $V_i(t)$. The difference between these velocities furnishes the rate of projectile erosion. Simultaneously, the metallic base moves at velocity of $V_b(t)$, and the difference between $V_b(t)$ and $V_i(t)$ gives the rate of penetration inside the fractured ceramic part (Fig. 1).

#### 2.2.1. Projectile erosion stage

In this region, the pressure in the projectile–ceramic interface is much higher than the yielding stress of the involved materials. As a result Tate [5,6] modified the hydrodynamic theory by introducing the dynamic yielding of the projectile ($Y_p$) and the resistance to ceramic penetration ($R_c$), both considered to be constants. Therefore, as the impact pressure increases and reaches the value $Y_p$, hence, the projectile will cease to act as a solid rigid body, and will be treated as a fluid subjected to the hydrodynamic laws. Similar behaviour will be applied to the target when it reaches the value of $R_c$.

The second stage starts when $t = 6(e_c/c)$, and the whole armour will participate in reducing the impact energy. Needless to say the rear part of the projectile moves at a velocity of $V_p(t)$, whereas, the projectile–ceramic interface moves with a velocity of $V_i(t)$. Simultaneously, the base will move at a velocity of $V_b(t)$, and

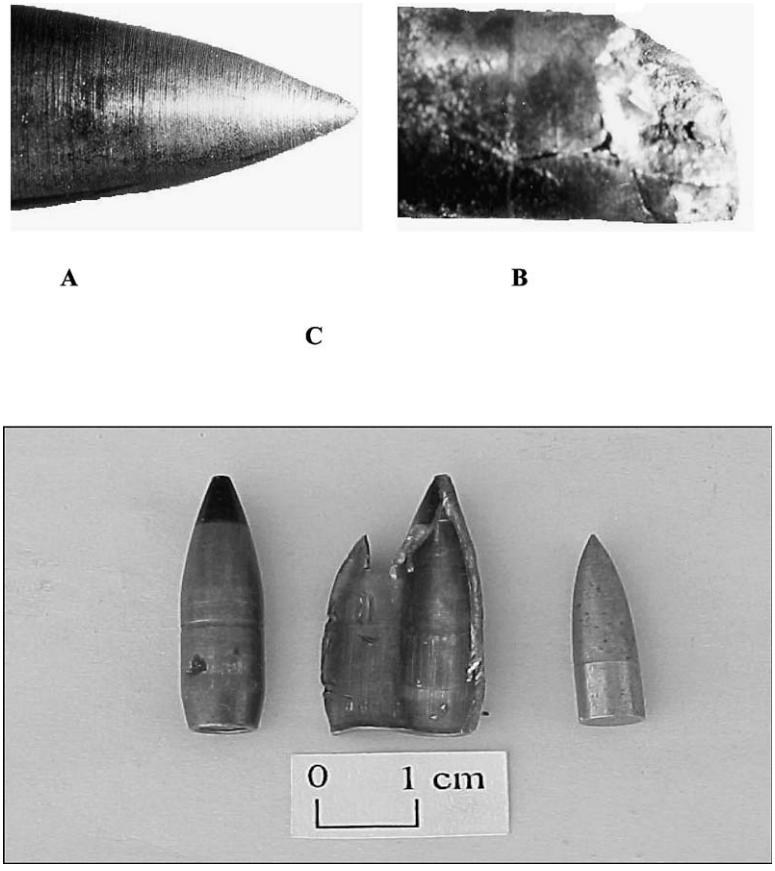


Fig. 2. Geometry of the projectile (A) before impact; (B) after impact in ceramic plate; and (C) steel nucleus.

will produce elastic deformation. However, the energy produced by this elastic energy will be small and will be neglected.

It is clear that as long as $V_p(t) > V_i(t)$, then the projectile is being eroded and losing mass and consequent reduction in the impact energy. The difference between these velocities furnishes the rate of projectile erosion, and also gives the velocity of penetration inside the fractured ceramic base. Fig. 4 shows the configuration of the process during the second stage. This can be expressed as

$$Y_p + \frac{1}{2}\rho_p(V_p - V_i)^2 = R_c + \frac{1}{2}\rho_c V_i^2, \tag{3}$$

where $R_c$ is the dynamic resistance strength against penetration into the ceramic.

Considering the first stage, then the deceleration of the projectile is given by

$$M_p \frac{dV_p}{dt} = -Y_p A_p, \tag{4}$$

where the initial velocity of the second stage coincides with the final velocity of first stage, because of the continuity condition. However, the reduction in the weight of the projectile is given by the following

$$\frac{dM_p}{dt} = -\rho_p A_p (V_p - V_i), \tag{5}$$

where the weight of the projectile at this stage is equal to that at the end of the first stage.

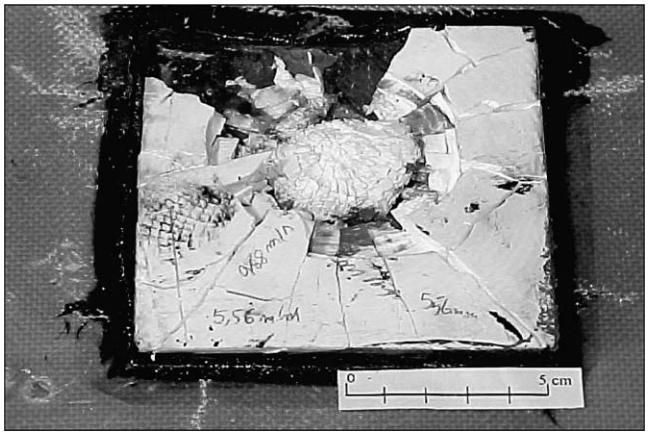


Fig. 3. Formation of fractured cone showing lateral spread of ceramic fragments.

### 2.2.2. Penetration with constant mass

During penetration it is possible that the velocity of the projectile $V_p(t)$ is equal to the interface velocity of

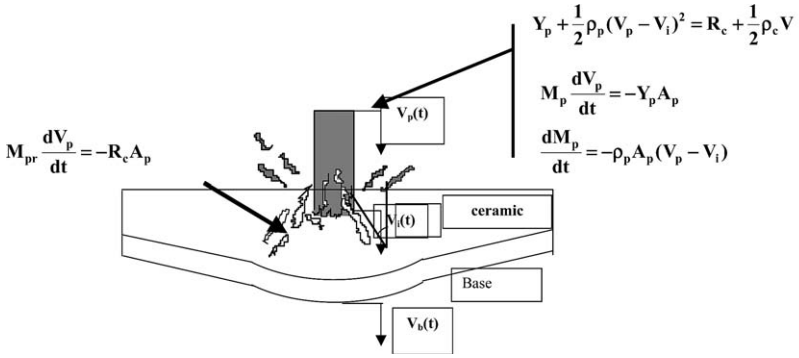


Fig. 4. Second stage penetration of the projectile, and elastic deformation of the base.

projectile–ceramic $V_i(t)$, which means the projectile is not eroding further and the mass is maintained constant. From this instant, Tate's hydrodynamic analogy becomes invalid, because the projectile and the interface move together at the same velocity. However, the rest of the projectile mass $M_{pr}$ continues to penetrate the completely fractured ceramic. Thus the force acting by the pulverized ceramic is given by

$$M_{pr}\frac{dV_p}{dt} = -R_c A_p. \tag{6}$$

### 2.2.3. Plastic deformation of the base material

In this final stage, the kinetic energy residual fragments of the projectile and the ceramic plate will be absorbed by the base material (stainless steel 304) which deforms plastically. Recently, Ishikura and Al-Qureshi [8,9], exhibited a typical exponential plastic deformation of the aluminium base plate caused by the impact of projectile of calibre 5.56 mm, as shown in Fig. 5. A mathematical model for determining the plate deflection, and the total plastic absorbed energy caused by the impact of the projectile was developed. Therefore it is possible to adapt their solution for the present work by assuming that the plastic energy is given by the residual projectile mass $M_{pr}$.

During the impact, the head of the projectile progressively penetrates the plate, thus causing a change in plastic deformation mode from indentation to bulging of the material. However, depending upon the speed of the projectile, the plate may not be perforated completely. In other words, simple penetration occurs, and the total plastic energy consumed by the plate to form a dimple shape on the plate can be expressed in terms of effective stress and strain as

$$E_p = \int_v \left( \int_0^{\bar{\varepsilon}} \bar{\sigma} \partial \bar{\varepsilon} \right) dV \tag{7}$$

For material with effective stress–strain curve of a power-law hardening expression $\bar{\sigma} = A(\bar{\varepsilon})^n$, then the

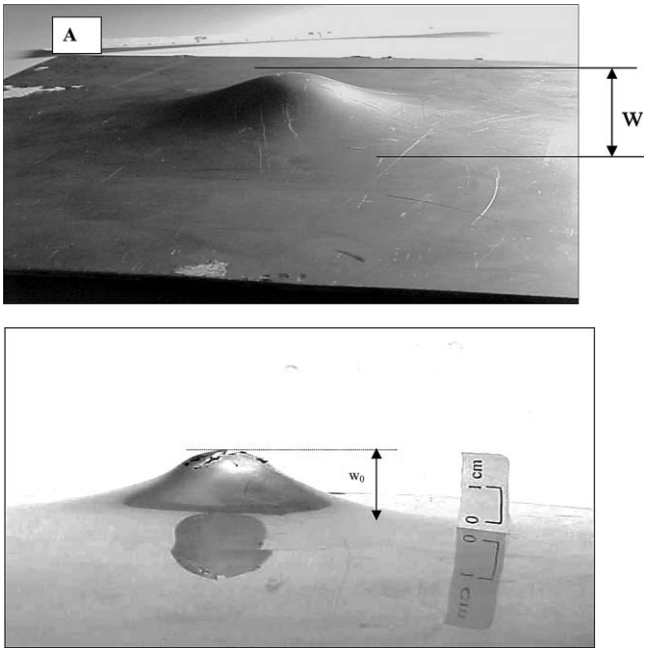


Fig. 5. Plastic deformation of metal base, maximum deformation is shown.

total plastic energy becomes

$$E_p = \frac{A}{n+1}\int_v (\bar{\varepsilon})^{n+1} dV. \tag{8}$$

Assuming the bulging of the material under the projectile impact force takes place in an axisymmetric mode, thus the effective strain can be written in terms of the radial strain as,

$$\bar{\varepsilon} = 2\varepsilon_r. \tag{9}$$

For small displacement, the radial strain can be approximated to [15,16],

$$\varepsilon_r = \frac{1}{2}\left(\frac{\partial w}{\partial r}\right)^2$$

thus,

$$\bar{\varepsilon} = \left(\frac{\partial w}{\partial r}\right)^2. \tag{10}$$

Also, from the geometry of the indentation due to impact, the volume of the small dimple can be expressed as

$$\mathrm{d}V = 2\pi r h \partial r, \tag{11}$$

where $h$ is the thickness of the plate. Substitution of Eqs. (10) and (11) into Eq. (9) gives

$$E_\mathrm{p} = \frac{2\pi h A}{n+1}\int_0^\infty \left(\frac{\partial w}{\partial r}\right)^{2(n+1)} r\partial r. \tag{12}$$

For the solution of the above equation, it is necessary to determine the plate deflection profile throughout the impact process of the projectile. However, from the present and previous experiments [9], it was found that the deflection profile can be expressed satisfactorily by an exponential form, and it can be described as follows

$$w = w_0 \exp\left[-\frac{kr}{D}\right], \tag{13}$$

where $w_0$ is the maximum deflection of the dome or dimple at $r = 0$, and $k$ is a deflection profile constant and can be determined experimentally. Substituting Eq. (12) into Eq. (13) gives

$$E_\mathrm{p} = \frac{2\pi h A}{n+1} \times \left(\frac{k w_0}{D}\right)^{2(n+1)} \int_0^\infty \exp\left\{-\frac{2kr(n+1)}{D}\right\} r\partial r. \tag{14}$$

The above equation can be integrated to yield the final expression for the total plastic energy absorbed by the plate and is given by

$$E_\mathrm{p} = B\left(w_0^{2(n+1)}\right), \tag{15}$$

where

$$B = \frac{\pi h A}{2(n+1)^3}\left(\frac{k}{D}\right)^{2n}.$$

On the other hand, the maximum deflection of the plate before perforation can be obtained by equating the total plastic energy, Eq. (15), to the kinetic energy of the projectile which is equal to

$$E_k = \frac{1}{2} m v_i^2 = E_\mathrm{p}. \tag{16}$$

It follows, therefore, that

$$w_0 = \left[\frac{m v_i^2}{2B}\right]^{\frac{1}{2(n+1)}}. \tag{17}$$

It becomes evident that the above expression is simpler than that derived by Calder and Goldsmith [14]. This, needless to say is due to simpler and more convenient choice of effective stress–strain relationship.

Considering the perforation of thin metallic plate where $e/D \leq 1$, then the plastic deformation energy is calculated from the projectile impact energy as

$$E_\mathrm{p} = \frac{1}{2} m\left(v_i^2 - v_r^2\right) - \frac{1}{2} v_r^2. \tag{18}$$

In fact, perforation and fracture of the plate occur when the material has reached its plastic instability, and the deformation has attained its maximum value. At this point the maximum effective strain can be calculated using Hill's membrane theory [15], and given by

$$\bar{\varepsilon} = \ln\left(1 + \frac{w_{0\max}^2}{a^2}\right), \tag{19}$$

where $a$ is the membrane radius. From the plastic instability theory, it can be calculated that the maximum effective strain at this point is simply given by [11,12],

$$\bar{\varepsilon} = n. \tag{20}$$

Experimental observations have shown that about 95% of the energy absorbed by the plate is dissipated in the initial deformation of the dimple within the membrane radius ($a$), which is approximately equal to four times the projectile radius ($D$). Therefore, from this approximation and substituting Eqs. (19), (20), into Eq. (15), the final expression for the energy absorbed by the plate as a result of projectile impact is given by

$$E_\mathrm{p} = \frac{\pi h A}{2(n+1)^3}\left(\frac{k}{D}\right)^2 \left\{4D\sqrt{\exp[n] - 1}\right\}^{2(n+1)}. \tag{21}$$

Close examination of the above equation, reveals that the absorbed energy is directly proportional to the plate thickness, and is greatly influenced by the work hardening characteristics of the material.

## 3. Experimental data and procedure

All the specimens were tested ballistically according to the MIL-STD-662E Standards [18–20]. The same projectile calibre was used throughout the whole experimental tests being $7.62 \times 51$ mm, and its initial velocity is approximately 835 m/s and 9.54 g, as shown in Fig. 6. The stainless steel 304 ($\bar{\sigma} = 935(\bar{\varepsilon})^{0.29}$ MPa, and density = 7.77 g/cm$^3$) had the following dimensions $30 \times 30 \times$ 1.5 cm over a ceramic base plate plate of $5 \times 5$ cm having different thicknesses of 7.3, 9.3 and 11.3 mm. In addition, a layer of aramide ply lined with sikaflex 221 resin was applied over the ceramic plate in order to retain the projectile fragments after each test. The character-

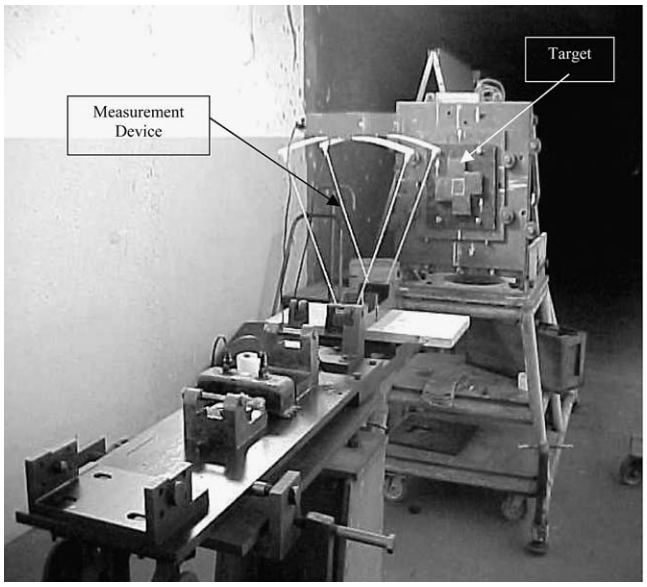


Fig. 6. Experimental set-up.

istics of the projectile employed and mechanical properties of the plate base are listed in Table 1 (Figs. 7–12).

The ceramic plates were manufactured from the same chemical composition, but having different grain sizes (TG). These were obtained by mixing different proportions of alumina calcinada A-1000SG and alumina T-60 (both are fabricated by Alcoa), and 2% of $TiO_2$ was added for the sinteriSation operation. Table 2 lists the two types of formulation used for these experiments.

The target made of ceramic–metal composite plates was attached to a special fixture to ensure a normal incidence of the projectile to the target. Special equipment was employed to measure the impact velocity, distance, time and other relevant information. Needless to say, the normal impingement of the projectile caused ceramic fracture and plastic deformation of the stainless steel base plate. After each test the maximum central deformation of the base ($w_0$) and the residual mass of the projectile ($M_{pr}$) were measured. These variables were used to determine the influence of the grain size on the efficiency and the penetration resistance of the analysed composite.

Table 1
Projectile properties

| Property | Steel nucleus of the projectile |
|---|---|
| Initial velocity (m/s) | 835.0 |
| Mass (g) | 9.54 |
| Vicker's hardness (HV) | 817.5 |
| Dynamic yield stress $Y_p$ (Gpa) | 2.82 |
| Density (g/cm$^3$) | 8.41 |

$$w_0 = \left(\frac{M_{pr}V_p^2}{2B}\right)^{\frac{1}{2(n+1)}} \qquad B = \frac{\pi e_b A}{2(n+1)^3}\left(\frac{k}{d_p}\right)^{2n}$$

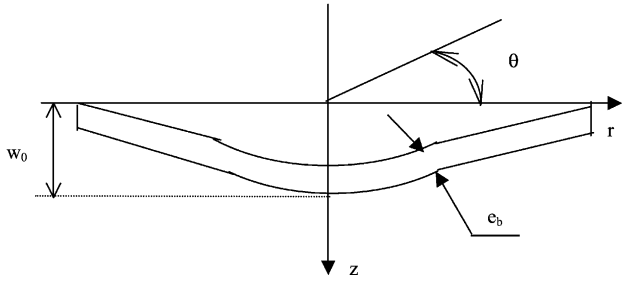


Fig. 7. Third stage plastic deformation of the metal base.

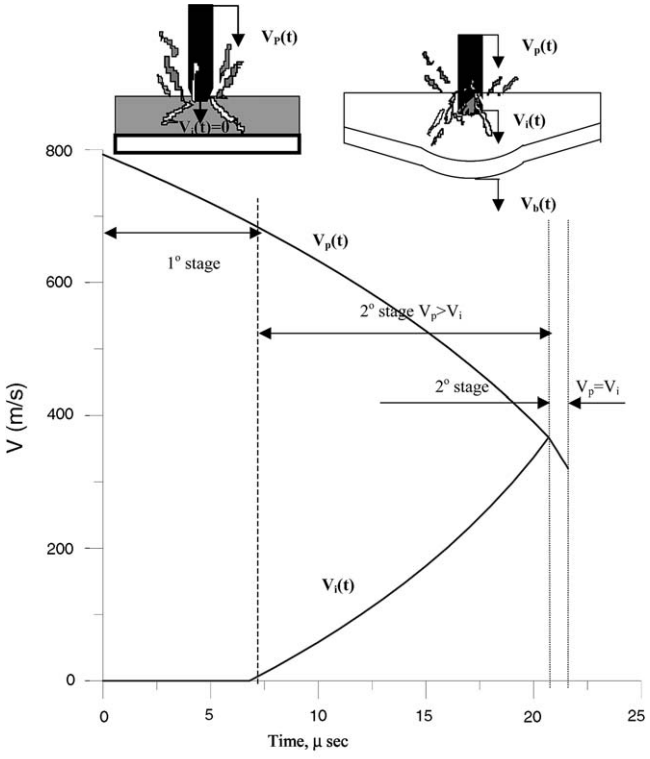


Fig. 8. Projectile velocity as a function of penetration time.

## 4. Discussion of results

### 4.1. Comparison between theoretical and experimental results

Normally, the kinetic energy is dissipated in eroding the impacting end when the conical-ended projectile of mass ($M_p$) impinges at normal bullet speed ($V_{i(t)}$). This fact causes a reduction in the speed before it can begin the penetration process of the ceramic plate. The impact of the projectile causes a concentrated zone of intense stress, thus forming a coronet fracture zone around the penetrating projectile Fig. 1.

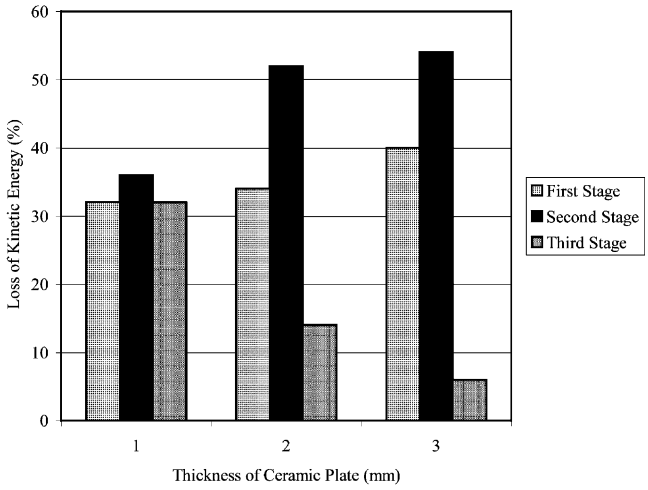


Fig. 9. Loss of impact energy as a function of ceramic plate thickness of different stages of penetration.

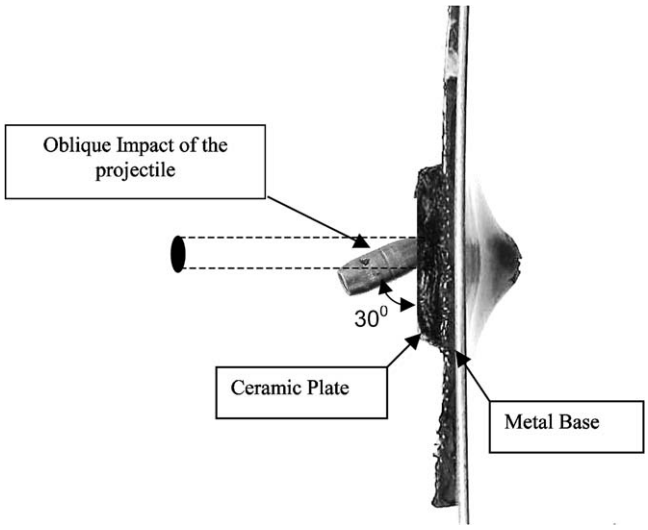


Fig. 12. Transversal section of projectile of oblique impact at 30°.

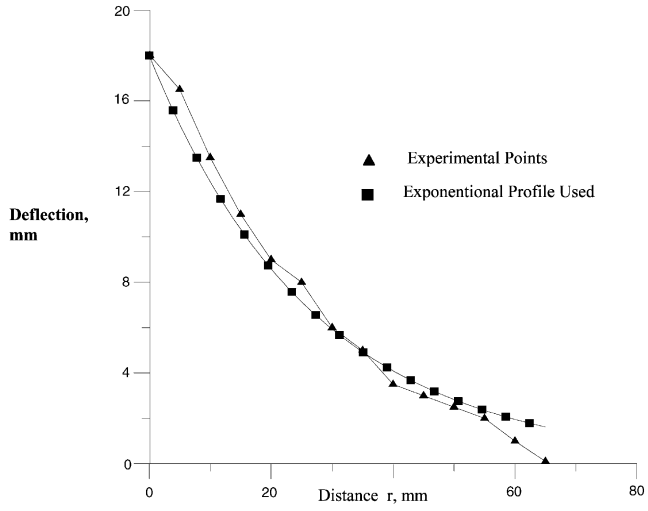


Fig. 10. Comparison between experimental and theoretical exponentional profile used.

Both the maximum deflection and the residual projectile mass were calculated theoretically and experimentally and this was performed on all tested materials of different thicknesses of ceramic plates. All these results are gathered in a simple form and enumerated in Table 3. Close examination of these values shows some evidence that predicted values by the present theory are generally in good agreement with the experimental results. The difference between the theoretical and the experimental results may be attributed to several factors such as the fact that the projectile does not impinge perpendicularly to the target, also the variation in the density and thickness of the ceramic plate. However the difference between the theoretical and experimental residual mass of projectile becomes more pronounced. This may be due to two factors. Firstly, the present theory considers that the transverse sectional area of the projectile remains constant, whereas Eq. (2) demonstrates that the loss of mass is directly proportional to the transverse sectional area. Since this area is assumed to be constant based on the calibre of the projectile, evidently the theoretical

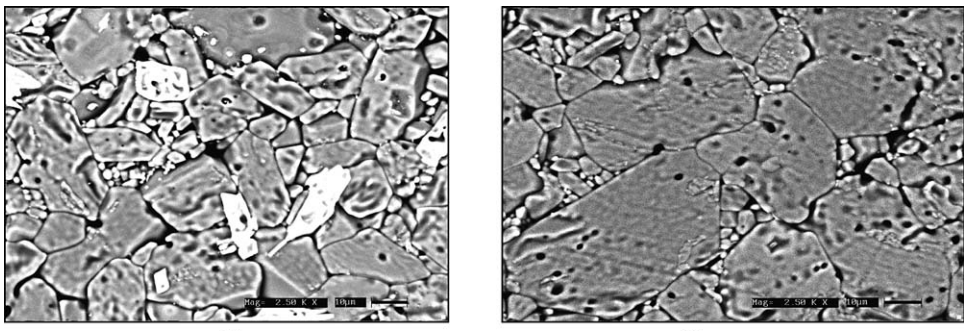


Fig. 11. Microstructrue of ceramic composition B and C.

Table 2
Ceramic plate composition

| Composition | $Al_2O_3$ A-1000SG (%) | $Al_2O_3$ tubular T-60 (%) | $TiO_2$ (%) |
|---|---|---|---|
| A | 95 | 3 | 2 |
| B | 90 | 8 | 2 |
| C | 85 | 13 | 2 |
| D | 80 | 18 | 2 |

loss of mass will be different from the experimental results, as demonstrated in Table 3. Secondly, during the experimental procedure, it was extremely difficult in many cases to distinguish between the fragments of the projectile and the fractured ceramics since they were mixed together after the ballistic impact. On the other hand, the theoretical model does not specifiy the minimum size of the fragments to be qualified as residual mass.

In spite of the many assumptions made in the present simple theory, it is clear however, that the results must not be taken as the absolute value, and several variables exist that will modify the estimated result.

### 4.2. Grain size effect

In general, from the present experimental results it was found that the ceramic composition which gives higher $V_{50}$ has the largest capacity to absorb impact energy caused by the projectile, thus having superior ballistic performance. $V_{50}$ is defined as the protection limiting ballistic velocity, which is equivalent to the velocity that causes partial or complete penetration of the projectile in the ceramic plate. Special measuring equipment was coupled with the experimental set-up to measure the various velocities of the projectile.

From the present investigation it was found that the ceramic of composition C (average grain size of 21.5 μm) had an average $V_{50}$, being higher by 5.8% than composition B (average grain size of 18.4 μm). This evidently indicates that the size of the grain has great influence on the absorbed ballistic impact energy, Table 4, thus, directly affecting the performance of the ceramic–metal composite armour behaviour.

Needless to say, more experimental results are needed before any final conclusion can be drawn with respect to the influence of grain size on the absorbing energy behaviour.

The difference between the two microstructures is clearly seen in Fig. 2. The mechanical properties of these compositions are listed in Table 4, from which it can be observed that there are great similarities. However, the only difference is the grain size where composition C has greater grain size than composition B, and this is due to the presence of a greater proportion of alumina.

### 4.3. Analytical results

The results of the present theoretical model with respect to the history of the theoretical velocities $V_p(t)$ and $V_i(t)$ during the first two stages of penetration are plotted in Fig. 3. It is worth mentioning that the residual impact energy absorbed during the third stage, which caused the plastic deformation of the base plate does not appear in Fig. 3. On close examination of the figure, it can be observed that the $V_i(t)$ stayed nil during the first stage because the projectile–ceramic interface remained stationary. On the other hand, during the second stage, while $V_p(t)$ decreases as penetration increases, the interface as from time $t = 20.5$ μs begins to increase steadily. However, when the two velocites become equal then both the projectile and the interface move together at the same velocity. Therefore, the erosion phenomenon ceases.

Considering the ceramic plates of 7.3 and 9.3 mm, the theoretical model predicts that the projectile velocity $V_p(t)$ is higher than the interface projectile ceramic velocity $V_i(t)$. This, needless to say, signifies that during the penetration into the ceramic plate, the projectile is being eroded constantly and its mass is reduced gradually as penetration proceeds. On the other hand, for ceramic of composition B (thickness = 11.3 mm) at the instant $t = 20.5$ μs, it is shown theoretically that $V_p(t) = V_i(t)$, thus no erosion takes place. As a result, from this point on, the projectile penetrates the ceramic

Table 3
Comparison between theoretical and experimental values

| Thickness of ceramic ($e_c$) (mm) | Composition | Impact velocity ($V_p$) (m/s) | Maximum deflection ($w_0$) (mm) | | |
|---|---|---|---|---|---|
| | | | Exp. | Theory | Error (%) |
| 11.3 | B | 792.7 | 16.5 | 17.0 | −2.9 |
| 11.3 | C | 858.2 | 20.0 | 17.6 | +13.6 |
| 9.3 | B | 628.9 | 18.0 | 17.8 | +1.1 |
| 9.3 | C | 651.1 | 17.5 | 17.7 | −1.1 |
| 7.3 | B | 428.8 | 15.5 | 17.3 | −10.4 |
| 7.3 | C | 448.4 | 13.0 | 16.6 | −21.7 |

Table 4
Summary of mechanical properties of various compositions

| Composition | A | B | C | D |
|---|---|---|---|---|
| Modulus of Weibull (m) | 14.4 | 8.4 | 8.8 | 15.1 |
| $\sigma_{50}$ (MPa) | 203.7 | 175.0 | 171.3 | 161.3 |
| $\sigma_0$ (MPa) | 209.0 | 182.8 | 178.5 | 165.2 |
| Vicker's Hardness (HV) | – | 1551.4 | 1259.8 | – |
| $R_c$ (GPa) | – | 4.43 | 3.60 | – |
| Density (g/cm$^3$) | 3.79 | 3.90 | 3.80 | 3.75 |
| Average grain size (μm) | – | 18.4 | 21.5 | – |
| Standard Error (μm) | – | 7.7 | 8.8 | – |

with constant mass, and the reduction in the velocity is caused mainly by the resistance force to penetration of the pulverized ceramic (Fig. 3). Despite the fact that the duration of the phase is very short (approximately 0.1 μs), the efficiency of considerably reducing the velocity of the projectile during penetration (approximately 50 m/s) is clearly indicated. On close examination of Fig. 3, it can be seen that the inclination $dV_p/dt$ during this phase is twice that of the inclination during the second stage.

It becomes evident that the importance of the reduction of the impact energy in each stage depends greatly on the the thickness of the ceramic plate employed for the armour composite. This fact can be demonstrated clearly in Fig. 4, where the second stage demonstrates the major part of the reduction of the projectile impact energy and increases with thickness of the ceramic plate. On close examination of Fig. 4, it can also be seen that for the plate thickness of 7.3 mm the loss of energy during the three stages is almost the same, about 33%. However, as the thickness of the ceramic plate increases, the reduction of the impact energy in the third stage reduces drastically and has almost no contribution, especially for thicker plates (about 10%). Therefore, it can be concluded that the design of the second stage plays the most important factor in reducing (over 50%) the ballistic impact energy.

## 5. Conclusions

The development of a simple and reliable theory to predict the loss of the ballistic impact energy absorbed by the armour plate was the main objective of the present work. It can also be concluded, despite the approximate nature of the analysis presented, that there is good agreement between the experimental and the theoretical results. In addition, the experimental results reported here demonstrate that composite ceramic–metal compete well with conventional materials.

The main advantage of the present model is the reduction in time during the phases of design and testing. Needless to say, it is a very effective tool to be employed in reducing the number of tests required for qualifying armour, since the cost of each is relatively high. In addition, other relevant parameters can be predicted, such as characteristics of the projectile, history of impact velocities, mechanical and geometrical properties of the ceramic and metal plates.

Finally, from the present theoretical and experimental results, it can be concluded that the thickness of the ceramic plate plays a major and fundamental role in the reduction or loss of the ballistic impact energy. Needless to say, it is also possible to modify other properties in order to reduce the impact energy without significant increase in the ceramic thickness. These may include the following factors which can be deduced from the present model:

1. The theoretical model demonstrates clearly that increasing the hardness of the ceramic will increase the resistance to penetration ($R_c$). As a result, during the second stage the mechanism of penetration becomes more effective thus reducing the velocity of projectile penetration.
2. The loss of impact energy during the third stage is $<10\%$. Therefore, the thickess of the base can be modified to participate effectively in the reduction of the impact energy.
3. Experimental results demonstrated that by increasing the grain size it is also possible to improve considerably the armour efficiency without increasing the ceramic thickness.

Today, police officers in most countries wear different kinds of body armour suitable for different operations. Kevlar is used in the manufacture of both bullet- and stab-proof armour worn by police/military forces. In bullet-proof armour, long strands of fibres form a dense net that absorbs the ballistic energy. Evidently the fibres must be able to distribute the whole impact force across the entire vest, ensuring that the impact force is not felt locally and intensely [17].

From the present experiments, it was demonstrated that armour can be reinforced by composite ceramic plates which are incorporated into a range of military vehicles, such as helicopters, where pilots are offered

armoured seats. These seats not only offer ballistic protection, but provide energy absorption [9].

Nowadays, there are several brands of fibres available, besides Kevlar, developed by DuPont, all offering different qualities, such as Dyneema, Twaron and Zylon.

## Acknowledgements

The authors wish to thank CTA and UFSC-LabMat for the use of the facilities and CAPES and CNPq for partially financing the project.

## References

[1] M.L. Wilkins, Mechanics of penetration and perforation, Int. J. Eng. Sci. 16 (1978) 793–807.
[2] M.L. Wilkins, Use of Boron Compounds in Lightweight Armor, Lawrence Livermore Laboratory, UCRL, 1978.
[3] M.L. Wilkins, M.W. Guinan, Impact of cylinders on a rigid boundary, J. Appl. Phys. 44 (3) (1973) 1200–1206.
[4] I.S. Chocron Benloulo, V.A. Sánchez-Galvez, New analytical model to simulate impact onto ceramic/composite armors, Int. J. Impact Engng. 21 (6) (1998) 461–471.
[5] A. Tate, A theory for the deceleration of long rods after impact, J. Mech. Solids 15 (1967) 387–399.
[6] A. Tate, Further results in the theory of long rod penetration, J. Mech. Phys. Solids 17 (1969) 141–150.
[7] W. Elber, Failure mechanics in low-velocity impacts on thin composite plates. NASA TP- 2152 (1983).
[8] D. Ishikura, H.A. Al-Qureshi, An investigation of perforation of metallic and composite plates by projectiles, Proc Fifth Pan American Congress of Applied Mechanics—PACAM V, San Juan, Puerto Rico, 5, 1997, pp. 194–197.
[9] D. Ishikura, H.A. Al-Qureshi, Study of perforation of metals and composite materials plates by projectile, Proc. XVth Physical Metallurgy and Materials Science Conference on Advanced Materials and Technology, Kraków-Krynica, Poland, 1998, pp. 544–547.
[10] R.L. Woodward, A simple one-dimensional approach to modeling ceramic composite armour defeat, Int. J. Impact Engng. 9 (4) (1990) 455–474.
[11] Z. Rosenberg, E. Dekel, A critical examination of the modified bernoulli equation using two-dimensional simulations of long rod penetrators, Int. J. Impact Engng. 15 (5) (1994) 711–720.
[12] J. Sternberg, Material properties determining the resistance of ceramics to high velocity penetration, J. Appl. Phys. 65 (9) (1989) 3417–3424.
[13] D. Tabor, The Hardness of Metals, Clarendon Press, Oxford, 1951.
[14] C.A. Calder, W. Goldsmith, Plastic deformation of thin plates resulting from projectile impact, Int. J. Solids Struct. 7 (1971) 863–881.
[15] R. Hill, The Mathematical Theory of Plasticity, Oxford University, Press, 1950, pp. 264.
[16] H.A. Al-Qureshi, J.D. Bressan, Investigation of the degree of biaxiality on the limit strains in sheet metal stretching, Proc. 9th The North Manufacturing Research Conf., NAMRC, SME, May, 1981, pp. 538–541.
[17] Anon. Defence, Fighting the bullets, Professional Engineeeering 16 (6) (2003) 28–29.
[18] Military Standard. $V_{50}$ Ballistic Test for Armor, MIL-STD-662E. Department of Defense, (1984).
[19] ASM, Mechanical Testing Handbook, 8, 1985, pp. 191–206.
[20] ASTM, Standard Test Method for Flexural Strength of Advanced Ceramics at Elevated Temperatures, C 1211 (1998).